FUNCTIONALISATION OF HUMAN CHLORIDE INTRACELLULAR ION CHANNELS IN MICROFLUIDIC DROPLET-INTERFACE-BILAYERS

Yu Zhang[a], Hazel Bracken[b], Cheryl Woolhead[b] and Michele Zagnoni[a]

[a] *Centre for Microsystems and Photonics, EEE Dept., University of Strathclyde, UK*

[b] *College of Medical, Veterinary & Life Sciences, University of Glasgow, Glasgow, UK*

Abstract Profiling ion flux through human intracellular chloride ion channels using live-cell based techniques, such as patch-clamp electrophysiology, is laborious and time-consuming. The integration of scalable microfluidic systems with automatable protocols based on droplet-interface-bilayers (DIBs) within which ion channels are incorporated circumvents several limitations associated with live-cell measurements and facilitates testing in controllable *in vitro* conditions. Here, we have designed and tested novel microfluidic layouts for the formation of arrays of DIBs in parallel and developed the first example of a miniaturised, DIB-based, fluorescence assays for Cl^- fluxing, allowing the investigation of the functional properties of the human chloride intracellular ion channel 1 (CLIC1). The microfluidic protocols relied on passive geometries for droplet pairing and DIB formation. Using recombinantly expressed CLIC1, we identified the best conditions to maximise protein integration into a lipid bilayer and the oligomerisation of the protein into functional ion channels. Finally, CLIC1 ion channel functionality was assessed relative to α-Haemolysin into microfluidic DIBs using the same Cl^- fluxing assay.

Keywords: microfluidics, droplet interface bilayers, chloride ion channels

Introduction

Ion channels are well recognised as central therapeutic targets for treating numerous pathophysiologies (Bagal et al. 2013). Established practise in large pharmaceutical companies for screening the effects of compounds on ion channels is to use automated, fluorescence-based, high-throughput assays, to monitor changes in membrane potential or intracellular ion concentration at the whole cell level, or automated patch-clamp technologies that monitor electrophysiological readouts mostly at the cluster channel level in live cells (Bruggemann et al. 2006; Clare 2010). These approaches require cloning and transfection of the target protein, which must be abundantly expressed in the chosen cell type. For ion channels, abundant

expression can be problematic, as levels substantially increased above physiological conditions can result in altered cellular homeostasis. Due to their inner-membrane locations, intracellular ion channels present additional screening difficulties.

CLIC1 is the best studied member of a family of 6 conserved proteins (CLIC1-6) in humans (Cromer et al. 2002). Due to their intracellular location, CLIC proteins have not been extensively studied. However, these proteins present an ideal model system to be studied *in vitro* as they have been shown to insert spontaneously into lipid vesicles, or artificial lipid bilayers, and form channels with properties similar to that seen *in vivo* (Tulk et al. 2000; Harrop et al. 2001). Recent discoveries have implied important roles for CLIC proteins in human diseases such as Alzheimer's, renal dysfunction and tumorigenesis, highlighting the importance of these channels in critical cellular activities.

CLIC1 proteins exist in a soluble form in the cytoplasm and undergo a large-scale structural rearrangement to self-insert into an inner membrane (Goodchild et al. 2011). CLIC1 insertion is controlled by pH, the oxidation status of the environment and the lipid composition of the membrane (Hossain et al. 2017). The CLIC1 monomer in the cytoplasm undergoes a rearrangement of the N-terminus GST-like domain to form an all-α-helical non-covalently bound dimer, induced under oxidising conditions (Littler et al. 2004). This structural re-arrangement involves the formation of an intra-molecular di-sulphide bond resulting in the exposure of a large hydrophobic domain, which is protected in this structure between the two dimer subunits. Exposure of this hydrophobic surface can serve to increase the ability of CLIC1 to dock with the membrane, as does the lower pH encountered at the membrane surface, which increase flexibility of the N-terminus thus promoting insertion (Goodchild et al. 2009). Oligomerisation and pore formation are thought to occur once CLIC1 has inserted, however understanding of this process is still relatively unclear.

Droplet microfluidic technology (Theberge et al. 2010) provides miniaturised methods for screening ion channels, creating high-throughput assays by handling and mixing nanolitre-picolitre amounts of drug compounds. The combination of droplet microfluidics with droplet-interface-bilayer (DIB) protocols (Schlicht and Zagnoni 2015; Trantidou et al. 2018) offers potentially large-scale solutions to overcome the limitations associated with the current live cell-based techniques, generating artificial cell membrane structures within which ion channels can be studied in simplified synthetic microenvironments (Bayley et al. 2008). Of importance when investigating ion channel functions in microfluidic DIBs is (i) the control over

droplet pair matching and positioning, (ii) guaranteeing automation of the microfluidic protocols and (iii) achieving large data throughput (Nguyen et al. 2016; Czekalska et al. 2019). This approach is therefore promising for studying intracellular ion channels, complementing life-cell electrophysiology data in situations where ion channel location or overexpression in live-cell is problematic.

Here, we present a scalable, microfluidic-DIB system for studying chloride ion channels. Recombinantly expressed, soluble CLIC1 was synthesized and tested off-chip to identify the assay conditions that maximized ion channel formation into artificial lipid bilayers. A miniaturised fluorescence assay based on a chloride sensitive dye indicator was developed to the test the functional behaviour of CLIC1 ion channels in microfluidic DIBs. This work had two overarching objectives: to develop a scalable microfluidic system capable of parallel DIB formation and simultaneous monitoring of ion flux across all DIBs via fluorescence-based assays; and to validate a novel multidisciplinary set of engineering and biochemistry methodologies for studying intracellular chloride ion channel 1 of the CLIC family. Overall, we show here the first example of a microfluidic DIB platform that demonstrates functionalisation of integrated human chloride ion channels.

Materials and method

Materials. List of materials, liposome and lipid preparation methods, as well as CLIC1 preparation method, are provided in Supplementary Information (SI).

Microfabrication and experimental setup. Microfluidic devices were fabricated in polydimethylsiloxane (PDMS) (Sylgard 184, Dow Corning, US) using standard soft lithography techniques and tested as previously described (Schlicht and Zagnoni 2015). (Details in SI).

Off-chip insertion assay. Liposomes were suspended in 20mM HEPES, pH 7.5 or pH 5.5 and CLIC1 protein added in a 3.4μM:12.5mM protein:liposome ratio (v/v), and incubated overnight at 4 °C. Samples were ultracentrifuged at 100,000 rpm for 1 hour at 4 °C and separated into supernatant and pellet fractions. Liposomes was re-suspended in 20mM HEPES, pH 7.5 or pH 5.5 buffer and passed through a 1 ml His-Gravitrap nickel affinity column (GE Healthcare), the column was washed with 2 column volumes 20mM HEPES, pH 8 and the flow through collected. The column was washed with 10 column volumes 20mM HEPES, pH 8, followed by elution of any protein bound to the column with 3 column volumes of elution buffer. Samples

were analysed through SDS-PAGE and Western blotting using a mouse anti-CLIC antibody (Abcam-ab77214).

BS^3 crosslinking. 0.5mM BS^3 crosslinker was added to both pellet and supernatant fractions and incubated at room temperature for 45 minutes. Unreacted BS^3 was quenched with 50mM Tris for 10 minutes at room temperature and samples analysed through SDS-PAGE and Western blotting. Similarly, for crosslinking of off-chip insertion assay products, 200 µL samples of pellet flow and elution fractions were crosslinked and analysed in the same way.

On-chip fluorescent assay. For DIB fluxing experiments with CLIC1 (120 µg/ml), 5 mg/ml 10:1 DOPC:cholesterol in hexadecane and alternating droplets containing non-fluorescent buffers (CLIC1, 10mM HEPES, 2mM H_2O_2, 200mM KCl, pH 5.5 - donor droplet) or fluorescent buffers (1.5 mg/ml SPQ, 10mM HEPES, 200mM KNO_3, pH 5.5 - acceptor droplet) were used. For DIB fluxing experiments with α-Haemolysin (2-20 µg/ml), 5 mg/ml DOPC or 4:1 DOPC:PC from soybean in hexadecane and alternating droplets containing non-fluorescent (10mM HEPES, 200mM KCl, α-Haemolysin, pH 7.4 - donor droplet) or fluorescent buffers (10mM HEPES, 200mM KNO_3, 1.5mg/mL SPQ, pH 7.4 - acceptor droplet) were used.

Results

Microfluidic architecture. A passive microfluidic design was developed to produce a 'flip-flop flow' of droplets in symmetric T-bifurcations (Fig. 1A). Two T-junctions generated two populations of phospholipid-stabilised, water-in-oil (W/O) droplets (one population encapsulating a buffer with the ion channel of interest and the other a buffer with a fluorescent reporter). The two trains of W/O droplets were serially arrayed in a serpentine channel leading to symmetric T-bifurcations (Video S1) where droplet flip-flop took place (Fig. 1A). When the first droplet arrived at a T-bifurcation, it randomly flowed to either the left or right channel. Subsequently, any other droplet followed the path of least fluidic resistance (Fig. 1B), with each droplet entering a new channel after the bifurcation and contributing to the change in resistance of the downstream channel network (Baroud et al. 2010). Interaction of neighbouring droplets at T-bifurcations enhanced the flip-flop sorting. Finally, after both trains of droplets had flown through the sorting channel network, droplet pair self-positioning (in AB configuration) was obtained in each droplet shift-register (Schlicht and Zagnoni 2015) (Fig. 1C) within which DIBs were formed (Fig. 1D). DIBs were formed within a few seconds of each other

and were incubated within the registers for the desired assay duration. Unwanted droplets were directed to a waste port (outlet1, Fig. 1A) using a manual valve. This approach provided high accuracy of droplet pairing and subsequent DIB formation (~97%). Therefore, the design was scaled up, achieving working configurations hosting 8, 16 (video S2) or 32 DIBs (Video S3) simultaneously.

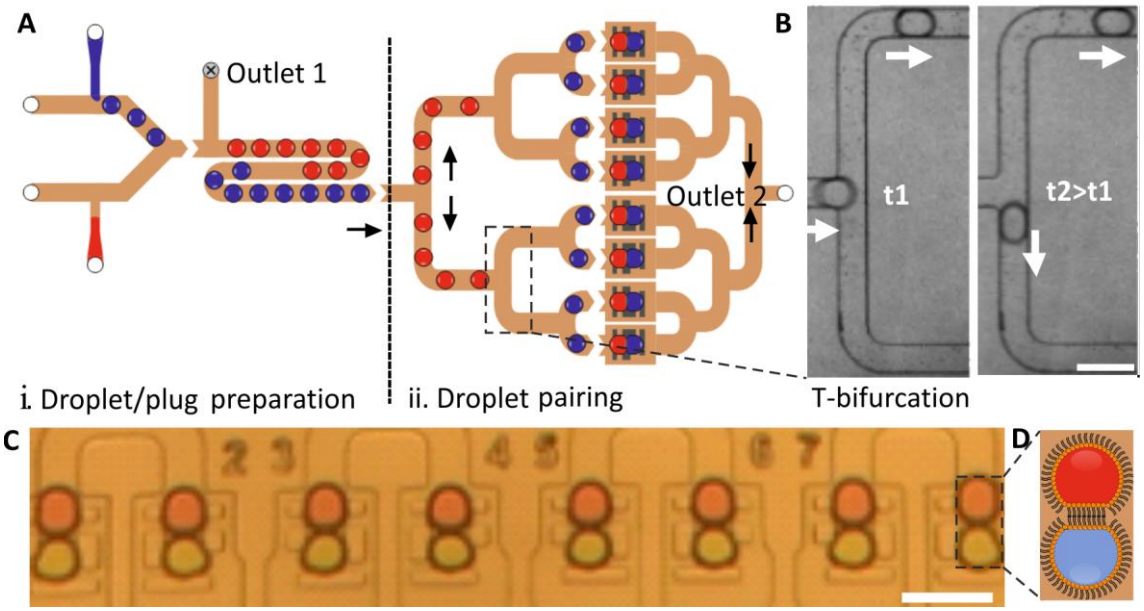

Figure 1. Microfluidic channel network designs for DIB formation. *(A) Symmetric T-bifurcations were used to obtain a 'flip-flop flow' of droplets at each bifurcation, where sorting took place (B). (C) Droplets arrayed in pairs forming DIBs (D) within droplet shift register traps. Scale bar 200 µm.*

A second geometry based on droplet splitting in symmetric Y-bifurcations (Fig. S1 and Video S4 in SI) was also developed. However, this resulted in more complicated protocols, leading to higher accuracy of droplet pairing (~100%), but also to frequent droplet pair coalescence and was therefore not developed further (details in SI).

Validation of microfluidic DIBs. Before testing CLIC1 channel functionality, a fluorescence-based assay was developed for the characterization of Cl^- ion fluxing using a chloride sensitive dye. This was validated in DIBs using the pore forming protein α-Haemolysin (α-HL) using different concentrations of α-HL and of its blocker gamma cyclodextrin (γ-CD)(Gu et al. 1999). α-HL is a lipid bilayer spanning toxin which forms a heptameric beta-barrel structure (Kawate and Gouaux 2003) and is permeable to small ions, such as Na^+, K^+, Ca^{2+} and Cl^- ions (Aksimentiev and Schulten 2005). The measurement of Cl^- fluxing relied directly on the change in intensity of a quinoline-based Cl^- fluorescent indicator, 6-methoxy-N-(3-sulfopropyl)quinolinium (SPQ).

SPQ is a lipid bilayer-impermeable dye that is quenched by halogen groups, such as Cl^- (Fig.2A), thus decreasing its fluorescence intensity for increasing concentration of Cl^-.

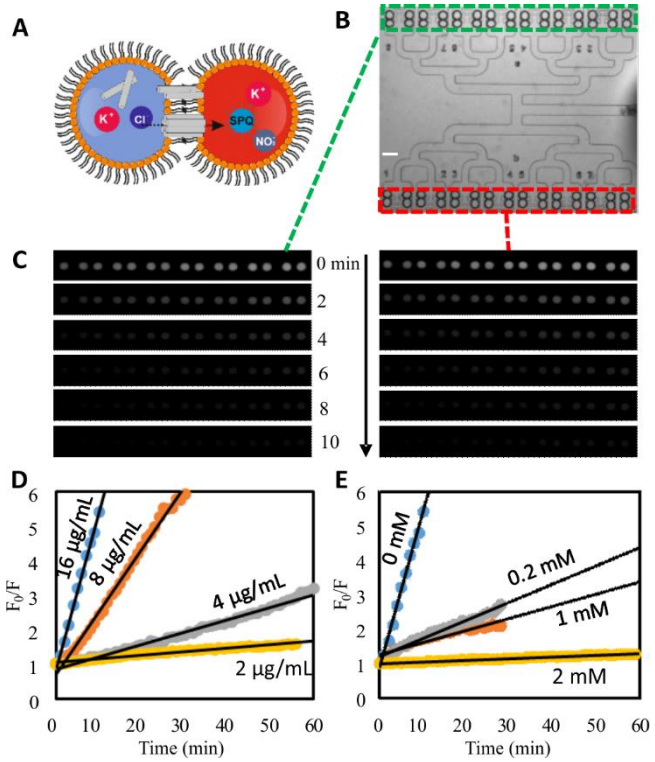

Figure 2. Cl^- fluxing fluorescence assay. *(A) A schematic representation of SPQ Cl^- fluxing through α-HL pores in DIBs. Donor droplet (left) and acceptor droplet (right). Upon fluxing of Cl anions from the left to the right droplet, the intensity signal from SPQ decreased over time. (B) Brightfield image of DIBs during the assay. Scale bar is 200 µm. C) Snapshots of the temporal evolution (from top to bottom) of the fluorescent signal in the acceptor droplet due to Cl^- fluxing. (D) Stern-Volmer plot of Cl^- fluxing with different concentrations of α-HL. (E) Stern-Volmer plot of Cl^- fluxing for different concentrations of γ-CD and a fixed concentration of α-HL. Black lines are a linear square fit of the experimental points for each protein or blocker concentration.*

Arrays of droplets in acceptor-donor pairs were formed within each droplet shift register trap, with one droplet encapsulating α-HL in a Cl^- buffer and its neighbour containing SPQ in an isosmotic Cl^- free buffer (Fig. 2A). The change in fluorescent intensity was monitored immediately after DIB formation for 10-60 minutes. α-HL monomers are known to oligomerise into a heptamer on the membrane surface, then spontaneously insert into the bilayer, forming ion channel pores (15-45 Å diameter) within DIBs. This allowed fluxing of Cl^- ions, but not SPQ molecules, quenching the dye over time (Fig. 2C-E). As a control, the same experiment was performed with donor droplets not containing α-HL, showing no detectable decrease in fluorescence (not shown). The Stern-Volmer relationship was used to estimate the quenching rate for varying concentrations of Cl^- (Illsley and Verkman 1987) (Fig. S2A in SI). Increasing concentrations of α-HL (2, 4, 8 and 16 µg/ml) produced faster fluxing of Cl^-, likely due to the greater number of α-HL pores being formed (Fig. 2D) in a DIB. γ-CD, a cyclic oligosaccharide

that reversibly binds to functional α-HL pores and transiently obstructs the ion channel pore, was used at different concentrations to reduce the Cl^- fluxing through α-HL (16 μg/mL) ion channels. As expected (Fig. 2E), higher concentrations of the blocker progressively decreased the rate of fluxing of Cl^- across α-HL pores in the DIBs.

Off-chip characterization of CLIC1 insertion into lipid bilayers. Metamorphic CLIC1 has been shown to form an all-α-helical non-covalently bound dimer under oxidising conditions (Littler et al. 2004), while lower pH has been shown to influence the stability of CLIC1, destabilising the N-terminus and exposure of the hydrophobic region, which in turn primes it for insertion to the membrane (Goodchild et al. 2009). To understand the oligomerisation mechanisms of CLIC1 upon insertion into the membrane, we incubated CLIC1 with liposomes at both pH 7.5 and pH 5.5 under both oxidising (2 mM H_2O_2) and reducing conditions (2 mM DTT). Ultracentrifugation was used to separate liposomes and bound protein into the pellet fraction, whilst any free protein remained in the supernatant fraction. BS^3 crosslinker was added to determine the oligomerisation of CLIC1 by covalently linking monomers, thus enabling visualisation on SDS-PAGE. In reduced conditions, CLIC1 remained as a monomer at both pH 7.5 and pH 5.5 in the absence of liposomes (Fig. 3A&B; Lane 10) and in the presence of liposomes in both the pellet and supernatant fractions (Fig. 3A&B; Lanes 11&12). However, in oxidising conditions at pH 7.5 CLIC1 existed as both monomers and dimers in the complete absence of liposomes (Fig. 3A; Lane 4) and also when bound to liposomes (Fig. 3A; Lane 5). but interestingly not in the supernatant, which, whilst also containing free CLIC1, only contained monomers (Fig. 3A; Lane 6). This indicates that it is only under oxidising conditions at pH 5.5 that CLIC1 exists in higher oligomeric structures, both free in solution (Fig. 3B; Lane 4) and bound to liposomes (Fig. 3B; Lane 5) where, as well as the presence of CLIC1 monomer, there are also bands corresponding to the presence of dimer, trimer, tetramer and other higher order structures. In the supernatant fraction, there exists only monomeric CLIC1 (Fig. 3B; Lane 6).

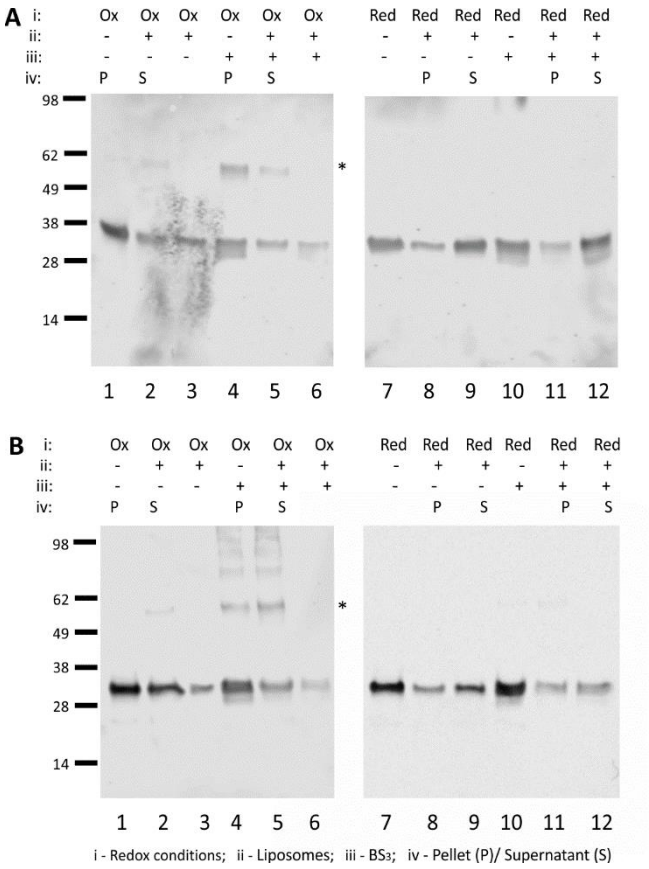

***Figure 3. CLIC1 oligomerisation analysed by BS^3 crosslinking**. Western blot analysis of BS^3 crosslinking experiments at (A) pH 7.5 and (B) pH 5.5 under oxidising (2 mM H_2O_2) and reducing (2mM DTT) conditions, detected by anti-CLIC1 antibodies. Pellet (P) - liposomes and bound protein, and supernatant (S) - free protein fractions. The CLIC1 monomer is ~30 kDa. (*) indicates dimer formation.*

To further test CLIC1 insertion, we developed a purification technique to isolate only liposomes containing inserted CLIC1 protein. When incubated with liposomes, the CLIC1 protein will insert with the N-terminus contained with the interior of the liposome and the C-terminus remaining exposed (Fig. 4A) (Tonini et al. 2000). The His-tag located at the N-terminus of the CLIC1 construct would be protected within the liposome.

Following ultracentrifugation, insertion of CLIC1 into DOPC liposomes was confirmed by applying the resulting fractions to His-Gravitrap nickel affinity columns. If CLIC1 was inserted into the liposomes, the His-tag will be located within the liposome and the protein and liposomes will pass through the column, collected in the initial 'flow-through sample'. Instead, if the latter is bound to the outside of the liposome or free in solution, it will bind to the column and only be released by addition of elution buffer, collected in the 'elution sample' (Fig. 4B). Results were visualised by SDS-PAGE and Western blotting (Fig. 4C). CLIC1 was only present in the flow-through sample in the pellet fraction under oxidising conditions at both pH 7.5 and pH 5.5, indication that CLIC1 is inserted in the liposome and therefore able to pass through the

column (Fig. 4C; Lanes 1&9). CLIC1 was also eluted from the nickel-column in the pellet fraction at both pH 7.5 and 5.5 (Fig. 4C; Lanes 2&10), suggesting that not all the CLIC1 is inserted to the membrane and some is associated to the outside of the liposome. At pH 7.5, there was also some CLIC1 in the elution fraction of the oxidised supernatant (Fig. 4C; Lane 4), whilst at pH 5.5 there was no detectable CLIC1 in the supernatant fraction in either the flow-through or elution (Fig. 4C; Lanes 11&12). Under oxidising conditions, the total level of insertion for pH 7.5 was calculated to be 11.5%, whilst pH 5.5 was 41.2% (Fig. 4C).

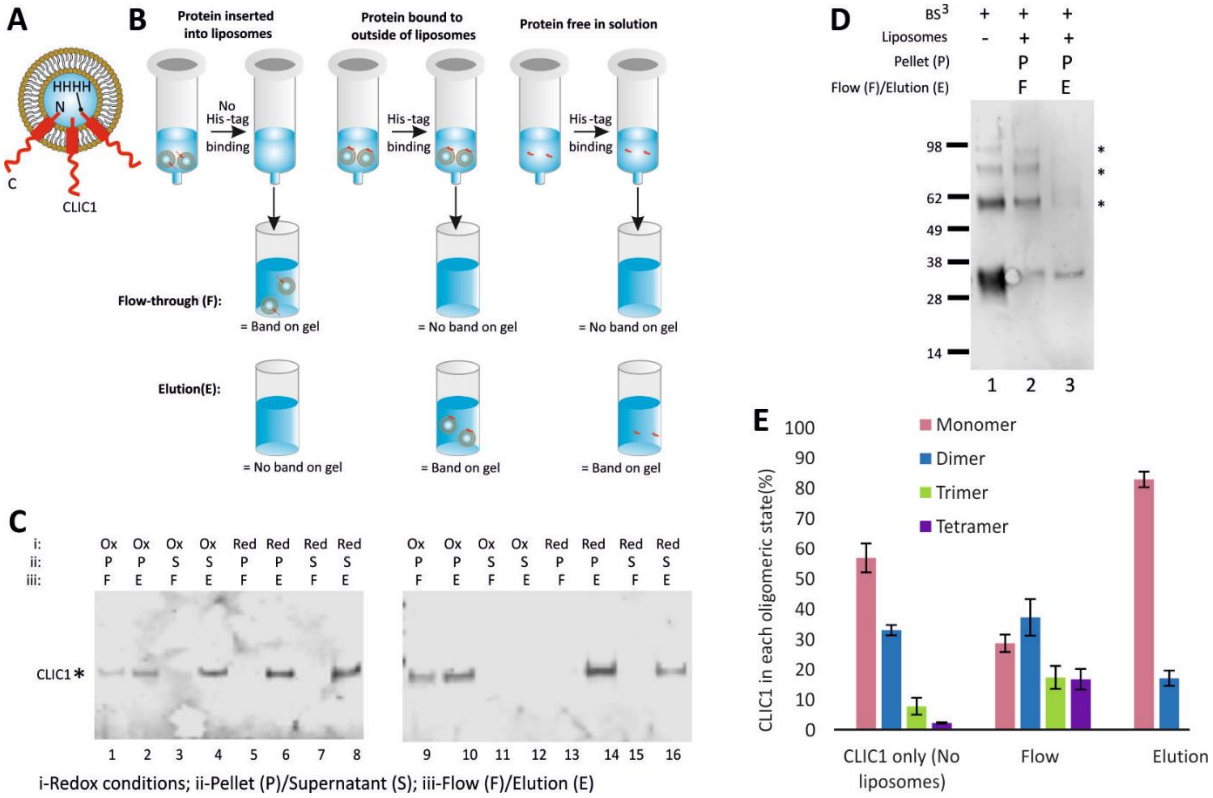

Figure 4. Analysis of CLIC1 insertion into DOPC liposomes. *(A) Schematic of CLIC1 inserted in a liposome. The N-terminus containing the His-tag is protected inside the liposome with the C-terminus exposed. (B) Schematic of the nickel column experiments to test CLIC1 insertion into liposomes. (C) Western blot analysis of nickel column experiments at pH 7.5 under oxidising (2mM H_2O_2) and reducing (2mM DTT) conditions, and pH 5.5 under oxidising (2mM H_2O_2) and reducing (2 mM DTT) conditions, detected by anti-CLIC1 antibody. (D) BS^3 crosslinking analysis of the Pellet Flow and Elution fractions under oxidising conditions (2mM H_2O_2) at pH 5.5 in comparison to CLIC1 protein free in solution in the absence of liposomes. (*) indicate oligomer formation. (E) % CLIC1 in each oligomeric state was calculated as a percentage of [Individual oligomeric state /Total protein for sample] with each value adjusted for background.*

In reduced conditions, CLIC1 was only found in the elution samples at both pH 7.5 and 5.5 in both the pellet and supernatant fractions, indicating that CLIC1 was not inserted and was only associated with the liposome in the pellet (Fig. 4C; Lanes 6&14) or free in solution in the supernatant (Fig. 4C; Lane 8&16).

Following this, the flow and elution samples at pH 5.5 under oxidising conditions were treated with BS^3 to determine the oligomerisation of CLIC1 inserted into liposomes (flow) and estimate the amount of CLIC1 bound to the outside of liposomes (elution). A lower proportion of CLIC1 inserted into the liposomes as a monomer, instead it predominantly existed as a dimer and other higher order oligomeric structures (Figure 4D; Lane 2). However, CLIC1 that was bound to the outside of the liposome predominantly existed as a monomer, with only a small proportion present as a dimer, with no evidence of any other higher order structures (Figure 4D; Lane 3). These experiments were repeated in triplicates (Fig. 4E) and image analysis showed that just under 60% of CLIC1 was present as a monomer in the absence of liposomes, with this figure reduced to just under 30% for CLIC1 inserted into liposomes and over 80% of CLIC1 bound to the outside of liposomes as a monomer. On average, over 35% of CLIC1 inserted into liposomes was present as a dimer, with approximately 15% of each existing as trimers and tetramers. Whereas, on average, approximately 15% existed as CLIC1 dimers bound to the outside of the liposomes with no other higher order structures detected.

Investigating functional pore formation of CLIC1. Having identified favourable conditions for CLIC1 insertion into lipid bilayers and characterised its oligomeric structures in liposomes, CLIC1 was tested in microfluidic DIBs to study the formation of functional CLIC1 chloride ion channels. Arrays of droplets in acceptor-donor pairs were formed within droplet shift-registers, with the donor droplet containing CLIC1 proteins. The change in fluorescent intensity was monitored immediately after DIB formation and recording was performed for at least ~90 minutes (Fig. 5). In the case of a functional CLIC1 pore, the fluorescent signal from the acceptor droplet decreased over time, with variable rate and duration. With respect to α-HL experiments where fluxing was observed in all experiments, CLIC1 yielded a success rate of ~5%, reflecting the outcome of the off-chip insertion experiments (15% of CLIC forming tetramers, most likely to be the functional form). This corresponds to approximately 5% of the total protein added being found as assembled membrane channels.

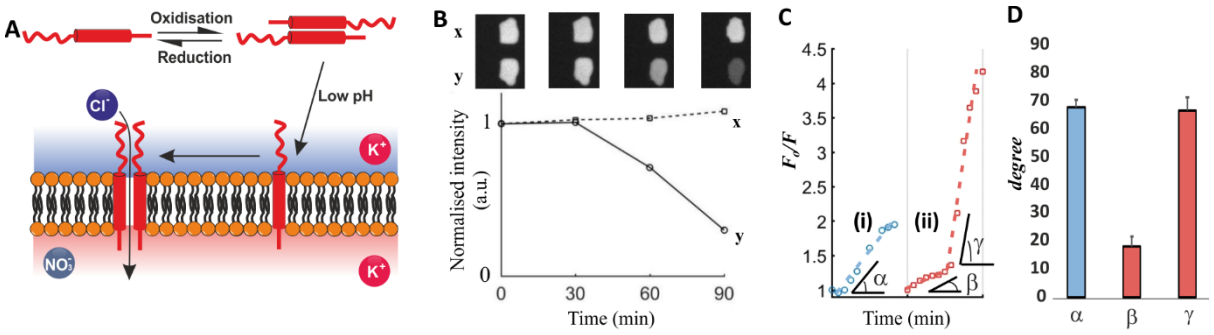

Figure 5. CLIC1 ion channel fluxing in DIBs. *(A) Schematic shows functional CLIC1 assembly into a lipid bilayer and consequent Cl^- fluxing. (B) Representative traces of fluorescent intensity from acceptor droplets (containing SPQ dye) in DIBs over 90 min acquisition period. Trace x shows sustained fluorescence signal in the case of no CLIC1 ion channel. Trace y shows decrease in fluorescence intensity due to a functional CLIC1 ion channels and Cl^- fluxing across a DIB. (C) Representative traces of two Cl^- fluxing behaviours in CLIC1 ion channels. (D) Difference between the two Cl^- fluxing behaviours in (C). Data shown as average value with standard errors.*

When testing CLIC1 functionality, the fluorescence intensity of the acceptor droplets was quenched at smaller rates than when using α-HL. Two distinct quenching behaviours (Fig. 5C&D) were identified in the Stern-Volmer plots of Cl^- fluxing: either an almost constant quenching rate (α in Fig. 5C(i)) or two almost constant quenching rates (β and γ in Fig. 5C(ii)), suggesting that either an increasing number of pores or different oligomeric states of the CLIC1 ion channel were present in the DIBs over time, consistently with previous reports using electrophysiology in live cells and planar lipid bilayers for CLIC1 (Warton et al. 2002, Costa et al. 2013).

Discussion

The proposed microfluidic architecture offers several advantages compared to others based on serial (Schlicht and Zagnoni 2015; Nguyen et al. 2016) or parallel (Czekalska et al. 2019) DIBs designs. These are: its scalability, the way DIBs can be formed within a few seconds of each other and the robustness of achieving droplet pairing in AB configuration and in parallel fashion. The parallel formation of DIBs is a particular advantage with respect to a serial architecture where, for increasing numbers of DIBs, a linearly increasing time lag is present between the first and the last DIB being formed, which impacts negatively when upscaling the platform. Importantly, the proposed architecture is free from droplet synchronisation strategies relying either on laborious tuning of droplet flows (Schlicht and Zagnoni 2015) or sophisticated geometries (Hong et al. 2010; Ahn et al. 2011; Xu et al. 2012; Gupta et al. 2011). With respect to these previous reports (stating 70% accuracy) (Bai et al. 2010), our approach produced better pairing efficiency (~97%) and the potential for more complex assays based on droplet packing

combinations (Fig. S3 in SI). Ultimately, larger versions of the proposed platform could offer a greater number of experiments carried out in parallel. With respect to electrophysiological measurement, this platform has potential to offer a cost-effective approach with greater throughput of information in exchange for poorer time resolution in ion channel response, thus complementing electrophysiology experiments. Therefore, this approach could be used in drug discovery for pre-screening large libraries of compounds, performing mechanistic studies and identifying hits, prior to more detailed electrophysiology measurements.

The Stern-Volmer equation can be rewritten (Eq. 7 in SI) as:

$$\frac{\boldsymbol{Fo}}{\boldsymbol{F(t)}} \cong \frac{[\boldsymbol{Cl^-}]_{\boldsymbol{D}}(\mathbf{0})}{\mathbf{2}} \cdot \frac{\mathbf{2}\boldsymbol{N} \cdot \boldsymbol{S} \cdot \boldsymbol{D} \cdot \boldsymbol{k_{vs}}}{\boldsymbol{V} \cdot \boldsymbol{L}} \boldsymbol{t} + \mathbf{1}$$

where *N* is the number of functional pores inserted into a DIB; *S* is the cross-section area of a pore; *D* is diffusion coefficient of the medium; C_o is the original concentration in the donor droplet; *L* is the length of the pore; V_a is the volume of the acceptor droplet. Considering negligible droplet shrinkage over the duration of the assay, *D,* C_o*, Kvs, V,* and *L* are constant throughout the experiment. The only parameters influencing the fluorescence quenching rate are *N and S*. For α-HL experiments, at each protein concentration (Fig. 2D), the rate of change of $F_o/F(t)$ *over time* was approximately constant, suggesting that the number of functional α-HL pores inserted into a lipid bilayer did not change over the course of the measurements. Whereas, for a fixed α-HL concentration, different γ-CD blocker concentrations affected the rate at which the section of the pore was blocked (Fig. 2E).

Results from the off-chip CLIC1 insertion assays indicate that CLIC1 only oligomerises to potential channel forming structures (trimers, tetramers and higher) under oxidising conditions at pH 5.5 (Fig. 3), confirming that low pH is essential for ion channel formation. The redox conditions also strongly influenced the efficiency of CLIC1 insertion into liposomes. Of the total CLIC1 that inserted into the liposome at pH 5.5 under oxidising conditions, the majority oligomerised (70%) (Fig. 4E), consistently with previous reports (Littler et al. 2004). Interestingly, despite having mixed monomers and oligomers under oxidising conditions in the absence of liposomes, in the presence of liposomes any CLIC1 that oligomerises becomes membrane bound. Essentially, this indicates that any CLIC1 undergoing the change to all- α-helical structure is able to insert into the membrane and oligomerise. Ultimately, these results account for the low insertion rates observed in the on-chip assays (Fig. 4E).

The latter result highlights the limitation of platforms based on lipid-bilayer harbouring ion channels, where channel insertion and its functional status is independent from the platform. This is a common issue in the literature, which limits many studies to the investigation of bacterial, spontaneously inserting ion channels. Our automated and simplified microfluidic approach facilitates the increase of data throughput in cases where low functional ion channel insertion is present.

Differences in flux rates are apparent between the CLIC1 experiments and those for α-HL. Firstly, α-HL will only integrate upon oligomerisation, therefore any membrane located protein will be found in a pore, whereas CLIC1 will integrate and then oligomerise to form a channel, resulting in multiple non-active membrane species. In addition, the α-HL pore is between 15 and 45 Å, whereas the CLIC1 channel is proposed to be between 1 and 5 Å. Furthermore, while the number of α-HL pores remained approximately constant for the duration of experiments, when testing CLIC1 two behaviours occurred. One where the pore size and number of pores remained approximately constant and one where a lower fluxing rate was observed prior to a higher one (Fig. 5 C&D). In our assay, when observing a change in fluxing rate, it is not possible to distinguish whether this was caused by an increase in the number of ion channels in the DIB or an increase in their pore size. Our results (Fig. 5D) suggest that, potentially, a higher oligomeric structure of the CLIC1 pore is obtained over time, reflecting the different levels of oligomeric structures observed in the off-chip assays (Fig. 4E). This finding compares well with previous electrophysiology reports of CLIC1 ion channels having a 'slow conductance slow kinetics' and 'high conductance fast kinetics' gating (Warton et al. 2002, Costa et al. 2013).

Conclusions

We have shown a novel microfluidic architecture, designed to simplify the automation of droplet-based operations, to precisely form DIBs and to assess the functionality of a membrane integrated ion channel, CLIC1. The performance of the microfluidic system for studying DIB processes was characterised and a novel fluorescence-based assay for studying Cl^- fluxing was developed together with a simplified analytical model of fluxing. The proposed paradigm, combining biochemistry procedures and scalable microfluidic assays, has the potential for creating powerful and efficient tools for cell-free drug screening of integrated membrane proteins, offering a cost-effective approach to analyse the function of intracellular ion channels and is amenable for use with a variety of ion channels.

Acknowledgements. The authors thank EPSRC (EP/N031849/1) for financial support.

Author Contributions. Y.Z. and M.Z. developed the microfluidic designs and assays; Y.Z. performed microfluidic experiments; H.B. and C.W. planned the CLIC1 off-chip insertion experiments, conducted by H.B.; Y.Z. and H.B. analysed the data; all authors participated to result discussion; all authors contributed to writing the manuscript.

Appendix A. Supporting information available. Supplementary data associated with this article can be found in the online version.

References

Ahn B, Lee K, Lee H, Panchapakesan R, Oh KW. 2011. Lab Chip 11, 3956-3962.

Aksimentiev A, Schulten K. 2005. Biophys J 88, 3745-3761.

Bagal S, Brown AD, Cox PJ, Omoto K, Owen RM, Pryde DC, Sidders B, Skerratt SE, Stevens EB, Storer RI et al. 2013. J Med Chem 56, 593-624.

Bai YP, He XM, Liu DS, Patil SN, Bratton D, Huebner A, Hollfelder F, Abell C, Huck WTS. 2010. Lab Chip 10, 1281-1285.

Baroud CN, Gallaire F, Dangla R. 2010. Lab Chip 10, 2032-2045.

Bayley H, Cronin B, Heron A, Holden MA, Hwang WL, Syeda R, Thompson J, Wallace M. 2008. Mol Biosyst 4, 1191-1208.

Bruggemann A, Stoelzle S, George M, Behrends JC, Fertig N. 2006. Small 2, 840-846.

Clare JJ. 2010. Targeting Ion Channels for Drug Discovery. Discov Med 9, 253-260.

Costa JA, Nguyen DA, Leal-Pinto E, Gordon RE, Hanss B. 2013. Plos One, 8 (5).

Cromer BA, Morton CJ, Board PG, Parker MW. 2002. Eur Biophys J Biophy 31, 356-364.

Czekalska MA, Kaminski TS, Makuch K, Garstecki P. 2019. Sensor Actuat B-Chem 286, 258-265.

Goodchild SC, Angstmann CN, Breit SN, Curmi PMG, Brown LJ. 2011. Biochemistry-Us 50, 10887-10897.

Goodchild SC, Howell MW, Cordina NM, Littler DR, Breit SN, Curmi PMG, Brown LJ. 2009. Eur Biophys J Biophy 39, 129-138.

Gu LQ, Braha O, Conlan S, Cheley S, Bayley H. 1999. Nature 398, 686-690.

Gupta R, Baldock SJ, Carreras P, Fielden PR, Goddard NJ, Mohr S, Razavi BS, Brown BJT. 2011. Lab Chip 11, 4052-4056.

Harrop SJ, DeMaere MZ, Fairlie WD, Reztsova T, Valenzuela SM, Mazzanti M, Tonini R, Qiu MR, Jankova L, Warton K et al. 2001. J Biol Chem 276, 44993-45000.

Hong J, Choi M, Edel JB, deMello AJ. 2010. Lab Chip 10, 2702-2709.

Hossain KR, Holt SA, Le Brun AP, Al Khamici H, Valenzuela SM. 2017. Langmuir 33, 12497-12509.

Illsley NP, Verkman AS. 1987. Biophys J 51, A514-A514.

Kawate T, Gouaux E. 2003. Protein Sci 12, 997-1006.

Littler DR, Harrop SJ, Fairlie WD, Brown LJ, Pankhurst GJ, Pankhurst S, DeMaere MZ, Campbell TJ, Bauskin AR, Tonini R et al. 2004. J Biol Chem 279, 9298-9305.

Nguyen MA, Srijanto B, Collier CP, Retterer ST, Sarles SA. 2016. Lab Chip 16, 3576-3588.

Schlicht B, Zagnoni M. 2015. Sci Rep. 5, 9951

Theberge AB, Courtois F, Schaerli Y, Fischlechner M, Abell C, Hollfelder F, Huck WTS. 2010. Angew Chem Int Edit 49, 5846-5868.

Tonini R, Ferroni A, Valenzuela SM, Warton K, Campbell TJ, Breit SN, Mazzanti M. 2000. Faseb J 14, 1171-1178.

Trantidou T, Friddin MS, Salehi-Reyhani A, Ces O, Elani Y. 2018. Lab Chip 18, 2488-2509.

Tulk BM, Schlesinger PH, Kapadia SA, Edwards JC. 2000. J Biol Chem 275, 26986-26993.

Warton K, Tonini R, Fairlie WD, Matthews JM, Valenzuela SM, Qiu MR, Wu WM, Pankhurst S, Bauskin AR, Harrop SJ, Campbell TJ, Curmi PMG, Breit SN, Mazzanti M. 2002. J Biol Chem, 277 (29), 26003-26011.

Xu LF, Lee H, Panchapakesan R, Oh KW. 2012. Lab Chip 12, 3936-3942.